Data-Driven Index Overlay and Boolean Logic Mineral Prospectivity Modeling in Greenfields Exploration

Mahyar Yousefi[1,3] and Emmanuel John M. Carranza[2]

Index overlay and Boolean logic are two techniques customarily applied for knowledge-driven modeling of prospectivity for mineral deposits, whereby weights of values in evidential maps and weights of every evidence map are assigned based on expert opinion. In the Boolean logic technique for mineral prospectivity modeling (MPM), threshold evidential values for creating binary maps are defined based on expert opinion as well. This practice of assigning weights based on expert opinion involves trial-and-error and introduces bias in evaluating relative importance of both evidential values and individual evidential maps. In this paper, we propose a data-driven index overlay MPM technique whereby weights of individual evidential maps are derived from data. We also propose a data-driven Boolean logic MPM technique, whereby thresholds for creating binary maps are defined based on data. For assigning weights and defining thresholds in these proposed data-driven MPM techniques, we applied a prediction-area plot from which we can estimate the predictive ability of each evidential map with respect to known mineral occurrences, and we use that predictive ability estimate to assign weights to evidential map and to select thresholds for generating binary predictor maps. To demonstrate these procedures, we applied them to an area in the Kerman province in southeast Iran as a MPM case study for porphyry-Cu deposits.

KEY WORDS: Data-driven, index overlay, Boolean logic, greenfields exploration, mineral prospectivity modeling.

INTRODUCTION

For mineral prospectivity mapping (MPM) for a certain deposit-type sought in a certain area, mineral exploration datasets used are based on a conceptual model of prospectivity of that deposit type. Then, from individual mineral exploration datasets corresponding evidential maps are generated, weighted, and integrated to delineate target areas. For this purpose, there are generally three approaches to assign weights to classes of evidential features in every map (Bonham-Carter 1994; Carranza 2008b). Evidential class weights can be assigned (1) based on the expert judgment of analyst through an approach called knowledge-driven MPM, for example, using index overlay and Boolean logic techniques (e.g., Bonham-Carter 1994; Carranza and Hale 2001; Carranza and Hale 2002b; Porwal et al. 2003c; Rogge et al. 2006; Carranza 2009), (2) by using the locations of known mineral occurrences as training points through an approach called data-driven MPM (e.g., Bonham-Carter 1994; Porwal et al. 2003a, b, c; Carranza 2008b), and (3) by using a hybrid of the two aforementioned approaches to MPM (e.g., Porwal et al. 2004, 2006; Carranza et al. 2008b). Traditionally, maps of spatially continuous evidential values (e.g., distance to structures, geological

[1]Faculty of Engineering, Malayer University, 65719-95863, Malayer, Iran.
[2]School of Earth and Oceans, James Cook University, Townsville, QLD, Australia.
[3]To whom correspondence should be addressed; e-mail: m.yousefi.eng@gmail.com

complexity, magnetic susceptibility, etc.) are usually firstly categorized into some classes using arbitrary intervals, and then all evidential values in each class are assigned using a technique that belongs to one of three mentioned approaches to MPM. This existing practice of categorizing spatially continuous evidential values for MPM is sensitive to the choice of class interval, and the relative importance of every value in a map is not really evaluated as evidence of mineral prospectivity.

Nykänen et al. (2008), Yousefi et al. (2012, 2013, 2014), and Yousefi and Carranza (2015) assigned weights to continuous-value evidential maps for MPM to overcome exploration bias in data- and knowledge-driven MPM resulting from simplification and discretization of evidential values into some arbitrary classes. In this technique, locations of known mineral occurrences are not used as training points, and spatially continuous evidential values (mainly distance to structures) are not discretized using arbitrary intervals. Although this technique addresses the foregoing issues in assigning weights to values in evidential maps, there are still issues in evaluating the relative importance of every evidential map derived from particular mineral exploration datasets. Assignment of meaningful weights to every evidential map is a highly subjective exercise and it usually involves a trial-and-error procedure (Carranza 2008b). Bonham-Carter (1994) proposed the index overlay method for knowledge-driven MPM, whereby classes of evidence in each evidence layer are assigned weights based on expert opinion and every evidential map is given a weight as well. There are other methods for knowledge-driven MPM that follows similar but different schemes of assigning weights to individual evidential maps using expert opinion as well. The applications of fuzzy logic (Carranza and Hale 2001; Porwal et al. 2003c, 2004, 2006; Lusty et al. 2012; Lisitsin et al. 2013) and the analytical hierarchy process (AHP) MPM approach (De Araújo and Macedo 2002; Moreira et al. 2003; Hosseinali and Alesheikh 2008; Najafi et al. 2014) have been demonstrated for knowledge-driven MPM. In that regard, one question is identified: is there data-driven way to assign weights that model the relative importance of every evidential map for MPM? To address this question, we propose a data-driven index overlay technique whereby, unlike the existing knowledge-driven index overlay technique, spatially continuous evidential values are assigned weights without discretization and individual evidential maps are assigned weights in a data-driven

way. In addition, we propose a data-driven Boolean logic MPM method whereby the selection of thresholds to convert every map of spatially continuous evidential values into binary predictor maps is based on data (i.e., using locations of known mineral occurrences). For this, we used the methods proposed by Yousefi et al. (2012, 2013, 2014) and Yousefi and Carranza (2015) to generate continuous weighted evidential maps. Then, for weighting individual evidential maps derived from particular mineral exploration datasets and for selecting thresholds to generate binary predictor maps for every set of continuous spatial values, the prediction-area (P-A) plot proposed by Yousefi and Carranza (2015) was used. While Yousefi and Carranza (2015) used the P-A plot only to evaluate prospectivity models, here we demonstrate that the P-A plot can be used to estimate the predictive ability of each evidential map with respect to known mineral occurrences, and that estimate of predictive ability can be used as (a) a weight of an evidential map and (b) for selecting thresholds to generate binary predictor maps. To demonstrate these procedures, we applied them to an area in the Kerman province in southeast Iran as a case study of prospectivity analysis for porphyry-Cu deposits.

METHODS AND RESULTS

Geology and Mineralization of the Study Area

The study area is a small part of the Urumieh–Dokhtar magmatic arc (Fig. 1a) forming the Zagros Mountains in Iran. These features are part of the Alpine–Himalayan orogenic belt, which resulted from the closure of the Neotethyan Ocean between Arabia and Eurasia (Sengor et al. 1988; Agard et al. 2005; Omrani et al. 2008). The protracted convergence history between Arabia and Eurasia comprised a long-lasting period of subduction followed by collision during the Tertiary (Omrani et al. 2008). Two magmatic belts dominated by calc-alkaline igneous rocks (Berberian and Berberian 1981) run parallel to the Main Zagros Thrust on the Eurasian upper plate and cut across central Iran. The magmatic activity was restricted to the Sanandaj–Sirjan magmatic arc and to the Urumieh–Dokhtar magmatic arc (Omrani et al. 2008). The Urumieh–Dokhtar magmatic arc, which is classified as an Andean magmatic arc (Alavi 1980; Berberian et al. 1982), forms an elongate volcano-plutonic belt running from eastern Turkey to south-
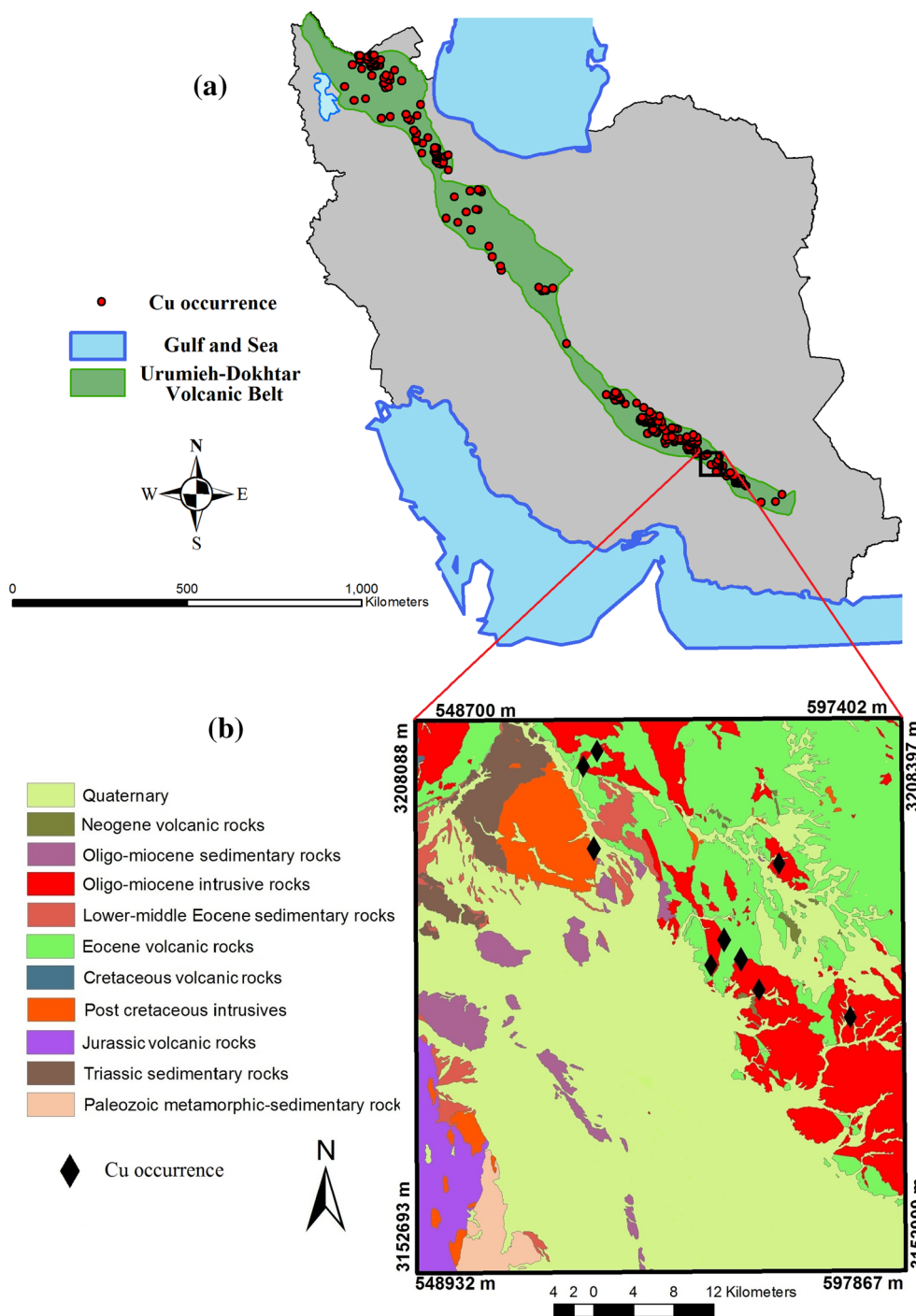
Figure 1. The Urumieh–Dokhtar volcanic belt and associated Cu occurrences in Iran (a), and simplified geological map of the study area (b).

east Iran and has been interpreted as subduction related (Takin 1972; Berberian and Berberian 1981; Berberian et al. 1982). Magmatism in the Urumieh–

Dokhtar magmatic arc occurred mainly during the Eocene but later resumed, after a quiescent period, during the Upper Miocene to Plio-Quaternary.

The Urumieh–Dokhtar magmatic arc has great potential for porphyry-Cu deposits (Fig. 1a) as far as its geology and exploration suggest (e.g., Tangestani and Moore 2002a, b; Hezarkhani 2006a, b; Atapour and Aftabi 2007; Boomeri et al. 2009). Some of the porphyry-Cu deposits in this magmatic arc that have been reported in the literature include the Sar Cheshmeh, Meiduk, Sungun, Chah-Firuzeh, and Reagan deposits (Hezarkhani 2006a, b, 2009; Boomeri, et al. 2009; Afzal et al. 2011). Unpublished reports by the National Iranian Copper Industries Company (NICICO) indicate that economically exploited porphyry-Cu deposits in the Urumieh–Dokhtar magmatic arc contain copper grades ranging from 0.15 to 0.8%. Associated igneous rocks vary in composition and are mainly granodiorites, quartz-diorites, diorites, diorite porphyry, granite-porphyry, monzonites, quartz-monzonites, and granites with ages of Cretaceous, Eocene, Oligocene–Miocene, and Neogene, which are spatially and genetically related to porphyry-Cu deposits in the Urumieh–Dokhtar magmatic arc. In this magmatic arc, volcanic rocks consist of mainly pyroclastics, trachy-andesites, trachybasalts, andesite-basalts, andesite lavas, tuffaceous sediments, dacites, rhyodacites, rhyolites, rhyolite tuffs, agglomerate tuffs, agglomerates, ignimbrites, basaltic rocks, and andesites with the age of Eocene and Neogene are spatially associated porphyry copper deposits, and some deposits are hosted by these volcanic rocks. In this paper, the study area measures ∼2,500 km^2 and is covered by the 1:100,000 scale quadrangle map of Sabzevaran prepared by the Geological Survey of Iran (GSI) (Grabeljsek 1956). The simplified lithostratigraphic map of the study area is shown in Figure 1b.

Conceptual Model of Porphyry-Cu Mineralization

Porphyry-Cu deposits are formed from post-magmatic hydrothermal fluids related to granitoid porphyritic intrusive rocks commonly having hydrothermal alterations (Arribas 1995; Singer et al. 2005). In porphyry-Cu deposits, primary ore minerals are dominantly structurally controlled and are spatially and genetically associated with felsic to intermediate porphyritic intrusions (e.g., Hezarkhani 2006a, b, 2009; Boomeri et al. 2009; Sillitoe 2010). Therefore, proximity to intrusive contacts (endo- and exo-contacts) represents favorability for porphyry-Cu mineralization (cf. Carranza and Hale 2002a, b; Carranza 2004; Qu et al. 2007; Carranza

et al. 2008a, b; Pazand et al. 2011; Yousefi et al. 2013; Lindsay et al. 2014; Yousefi and Carranza 2015). Porphyry-Cu deposits can be distinguished from other granite-related deposits such as skarns and mantos by their large size and structural control, mainly stockworks, porphyry stock, veins, vein sets, fractures, and breccias (e.g., Sillitoe 2010).

In the formation of porphyry-Cu deposits, once the magma solidifies, high-temperature fluids are released into the solidified porphyry and its surrounding host rocks. The fluids, which are often mineral-rich, take the path of least resistance and travel through cracks and fractures, which facilitate the passage of magmas and the circulation of hydrothermal fluids (cf. Sillitoe 1997; Hanuš et al. 2000; Roy et al. 2006). It is generally accepted that fault zones act as major channel ways for deeply sourced melts as well as hydrothermal fluids (Storti et al. 2003; Pirajno 2010). Fault architecture has been used to investigate porphyry systems as described in many studies worldwide (e.g., Guillou-Frottier and Burov 2003; Qu et al. 2007; Pirajno 2010; Chen et al. 2011), as well as in the Urumieh–Dokhtar belt of Iran (e.g., Ghasemi and Talbot 2006; Meshkani et al. 2013).

Porphyry-Cu deposits in the Urumieh–Dokhtar belt of Iran show geochemical halos of indicator elements mainly Cu, Mo, Au, Ag, Zn, Pb, As, and Sb (e.g., Ziaii et al. 2011; Yousefi et al. 2013; Yousefi and Carranza 2015).

Datasets: Weighted Evidence Layers

Based on the conceptual model of porphyry-Cu mineralization in the study area, geochemical signatures, faults/fractures, and proximity to intrusive rocks can be used as proxy evidence to predict this type of deposit. Thus, based on the conceptual model of porphyry-Cu mineralization and available mineral exploration datasets in the study area, we used three weighted maps of evidence of prospectivity for porphyry-Cu deposits, namely (i) distance to intrusive contacts (Fig. 2a), (ii) fault density (FD) (Fig. 2c), and (iii) multi-element geochemical signature (Fig. 2b), geochemical mineralization prospectivity index, $GMPI_{porphyry-cu}$ (Yousefi et al. 2012, 2014), calculated as indicator factor scores (FS) of the deposit-type sought. Each of these weighted evidential maps was generated and weighted by Yousefi and Carranza (2015) using logistic functions (Yousefi et al. 2012, 2013, 2014; Yousefi and Carranza 2015) with a pixel size of 100 m×100 m in all
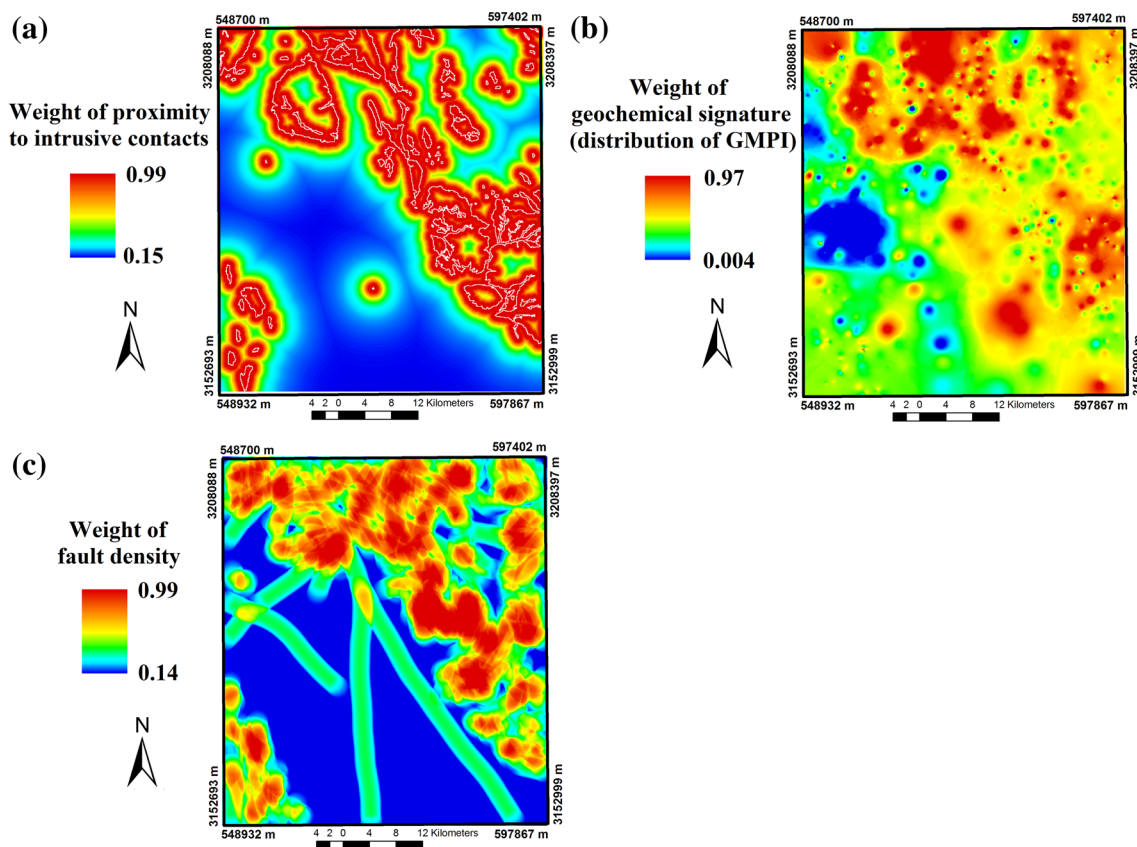
Figure 2. Continuous weighted evidence layer of (a) distances to intrusive contacts, (b) multi-element geochemical signature, map of GMPI$_{Cu\text{-}porphyry}$ values, and (c) fault density (from Yousefi and Carranza 2015).

of the maps stored in a GIS. This cell size was obtained by using the function of scale number recommended by Hengl (2006). As Nykänen et al. 2008, Yousefi et al. (2012, 2013, 2014), and Yousefi and Carranza (2015) have demonstrated, weighted evidential maps can be generated from spatially continuous values by using logistic functions without using the locations of known mineral occurrences and without simplification and discretization of evidential values into some arbitrary classes using expert judgment.

Data-Driven Assignment of Weights to Evidence Layers

In MPM, weights assigned to spatial evidence must reflect realistic spatial associations between spatial evidence and mineral deposits of the type sought. Therefore, the locations of known mineral occurrences can be used to evaluate the reliability of

weights assigned to spatial evidence representing their spatial associations with mineralization in the study area. This is achieved by overlaying the locations of known mineral deposits on a classified mineral prospectivity map (e.g., Porwal et al. 2003c, 2004, 2006; Carranza et al. 2005; Yousefi et al. 2012, 2013, 2014; Yousefi and Carranza 2015).

The fractal theory, which was introduced by Mandelbrot (1977, 1983) and Mandelbrot et al. (1984), has been applied to characterize and classify physical and chemical quantities with geometrical support. In the geosciences, fractal models have been used to explain the spatial distributions of geological features (e.g., Cheng 1995; Cheng and Agterberg 1995; Wang et al. 2006, 2008; Raines 2008; Carranza and Sadeghi 2014). Several fractal models have been developed and successfully applied to study spatial features related to mineralization (e.g., Panahi and Cheng 2004; Agterberg 2007; Carranza 2008a; Ford and Blenkinsop 2009; Gumiel et al. 2010; Afzal et al. 2011; Arias et al.
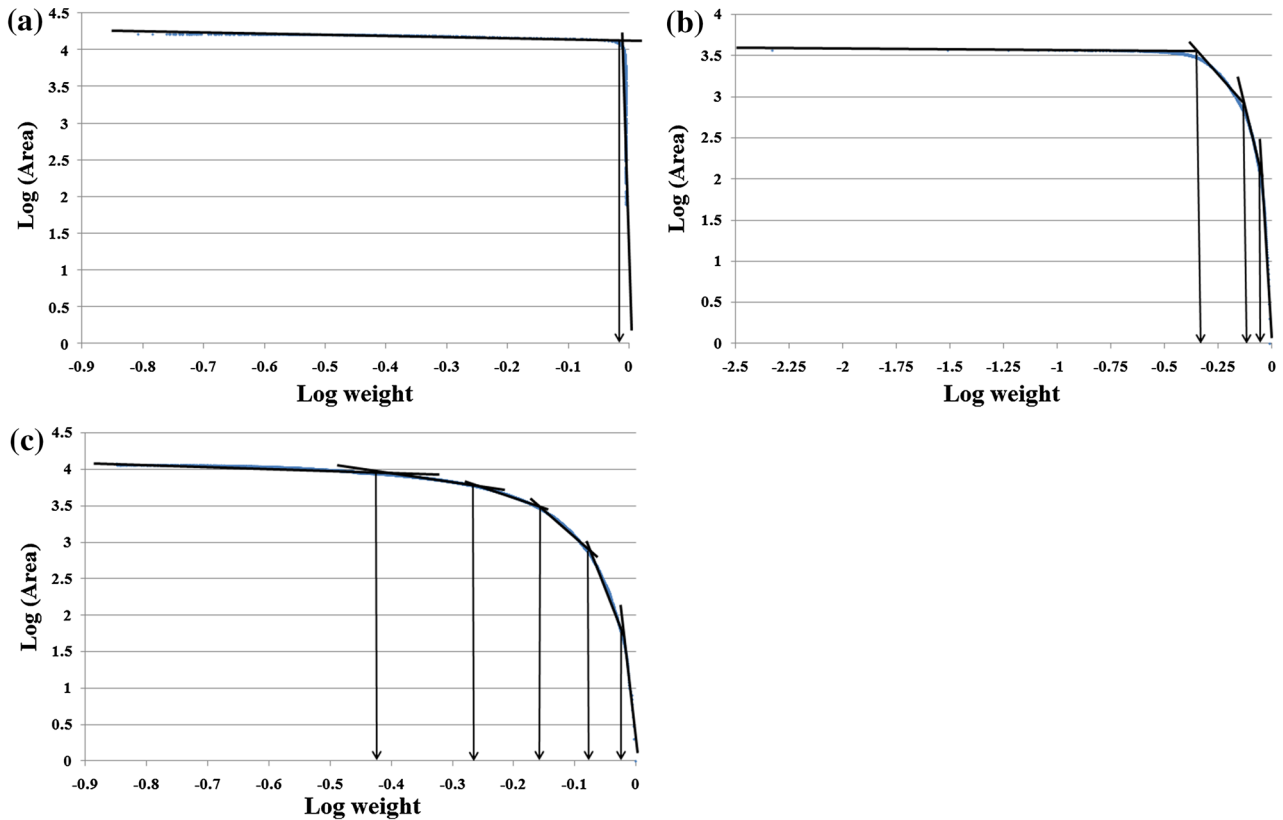
Figure 3. Concentration-area model, log–log plots for the weighted values of (a) distances to intrusive contacts, (b) multi-element geochemical signature, $GMPI_{Cu\text{-}porphyry}$ values, and (c) values fault density.

2011) such as geochemical anomalies (e.g., Cheng et al. 1994, 1996, 2010; Cheng 1999, 2007; Carranza 2008b, 2010a, 2010b, 2011; Zuo and Cheng 2008; Cheng and Agterberg 2009; Deng et al. 2009, 2010, 2011; Wang et al. 2011a; Zuo 2011a, 2011b, 2011c; Zuo and Xia 2009; Zuo et al. 2009b), structural controls (e.g., Carranza 2008a; Carranza et al. 2009; Carranza and Sadeghi 2010; Zhao et al. 2011), and geological controls (e.g., Ford and Blenkinsop 2008; Zuo, Agterberg, et al. 2009a; Wang et al. 2011b). Considering the foregoing literature, geological features (e.g., geochemical anomalies, fault distribution, etc.) have fractal dimensions. In this paper, we used the concentration-area (C-A) fractal model (Fig. 3a–c) proposed by Cheng et al. (1994) to determine thresholds for classifying values in evidential maps (Fig. 4a–c).

To evaluate and quantify the ability of each class of evidential features in predicting mineral deposit occurrences, the weights of classes of evidential features can be divided by the ratios of their areas to the total area studied. These ratios represent the predictive ability of each evidential class (cf.

Bayes 1764; Good 1950; Bonham-Carter et al. 1989; Jaccard 1908; Yule 1912). Therefore, if two different classes of spatial evidence with different areas have the same weight, the probability of finding undiscovered deposits is higher for spatial evidence covering smaller areas. In this regard, Yousefi et al. (2012, 2013) used a plot in which the classes of prospectivity were shown versus the percentage (prediction rate) of known mineral occurrences predicted by the corresponding prospectivity classes as a way to evaluate different prospectivity models. In a scheme to make P-A plots, Yousefi and Carranza (2015) used together the probability of known mineral occurrences predicted by prospectivity classes, and the areas occupied by the corresponding classes of prospectivity (with respect to the total study area). In this paper, we used the P-A plot to evaluate and to weight every evidential map (Fig. 5a–c). In a P-A plot for an evidential map, the intersection of the curves (1) the curve of prediction rate of known mineral occurrences corresponding to the classes of the weighted evidential layer, and (2) the curve of percentage of occupied areas
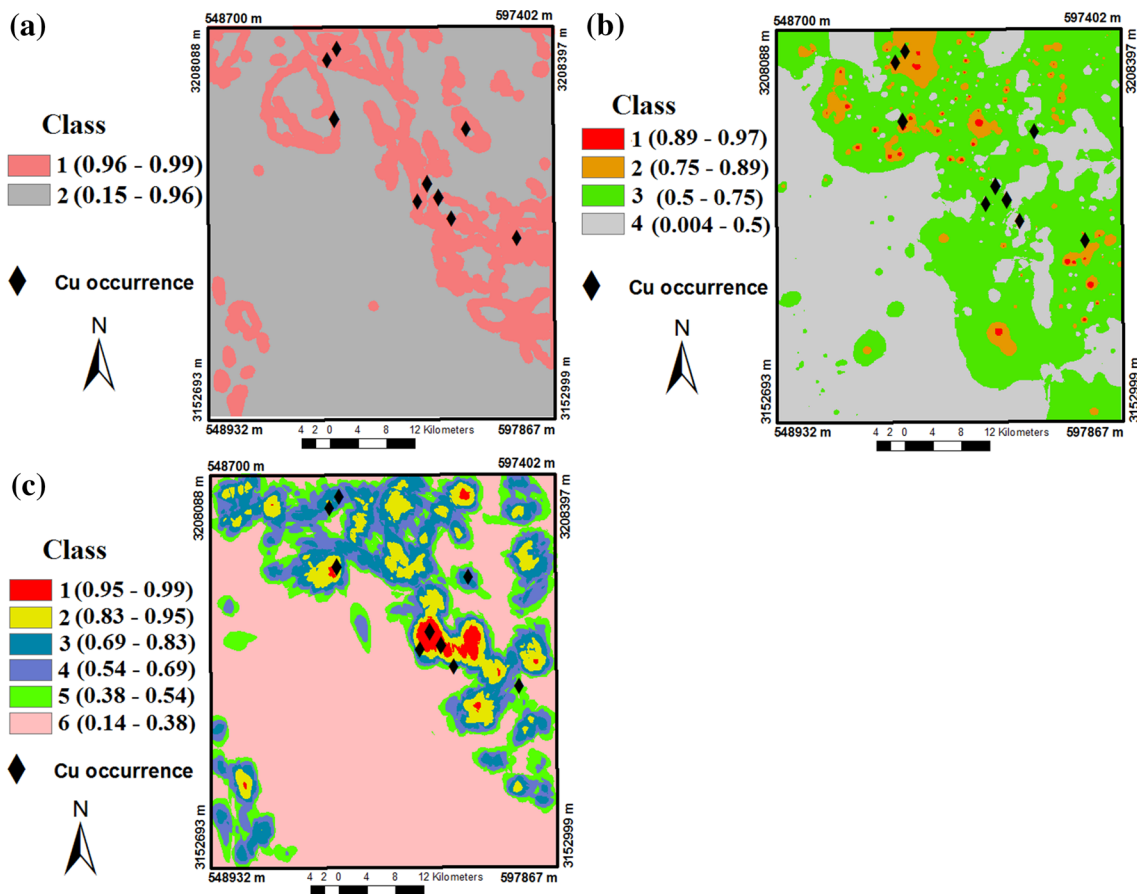
Figure 4. Classified weighted map of (a) distances to intrusive contacts, (b) multi-element geochemical signature, map of GMPI$_{Cu\text{-}porphyry}$ values, and (c) fault density.

corresponding to the classes of the weighted evidential layer, is a criterion for weighting and evaluating the predictive ability of that evidential map. If the two curves intersect somewhere in the P-A plot that is closer to the y-axis but farther from the x-axis, it represents a small area containing large number of mineral deposits and, thus, it means high probability of occurrence of mineral deposits. In a P-A plot for an evidential map, the X and Y values of the intersection point are used to extract meaningful parameters for MPM. The Y value (at left axis) is the prediction rate for the evidence layer and it is its weight to predict the deposit-type sought. The X value is a meaningful criterion to select threshold for creating a binary evidence map because a majority number of mineral deposits are associated with the range from X to the maximum values of evidence.

For the present study, the parameters of the intersection points in the P-A plots are shown in

Table 1 (extracted based on Fig. 5a–c for the individual evidential maps) and they quantitatively portray the order of evidential maps in terms of decreasing relative importance as (1) intrusive contacts, (2) fault density, and (3) GMPI. This order shows that in the study area: (a) intrusive contact, with a prediction rate of 86%, is the most important criterion of porphyry-Cu prospectivity because intrusives are heat sources for this type of mineralization and, thus, are genetically as well as spatially related with porphyry-Cu deposits; (b) fault density, with a prediction rate of 80%, for the second important criterion because faults provide flow pathways for hydrothermal fluids; and (c) GMPI, with a prediction rate of 69%, is the third important criterion because it is a significant multi-element anomalous signature derived from stream sediment dataset of indicator elements for porphyry-Cu deposits.
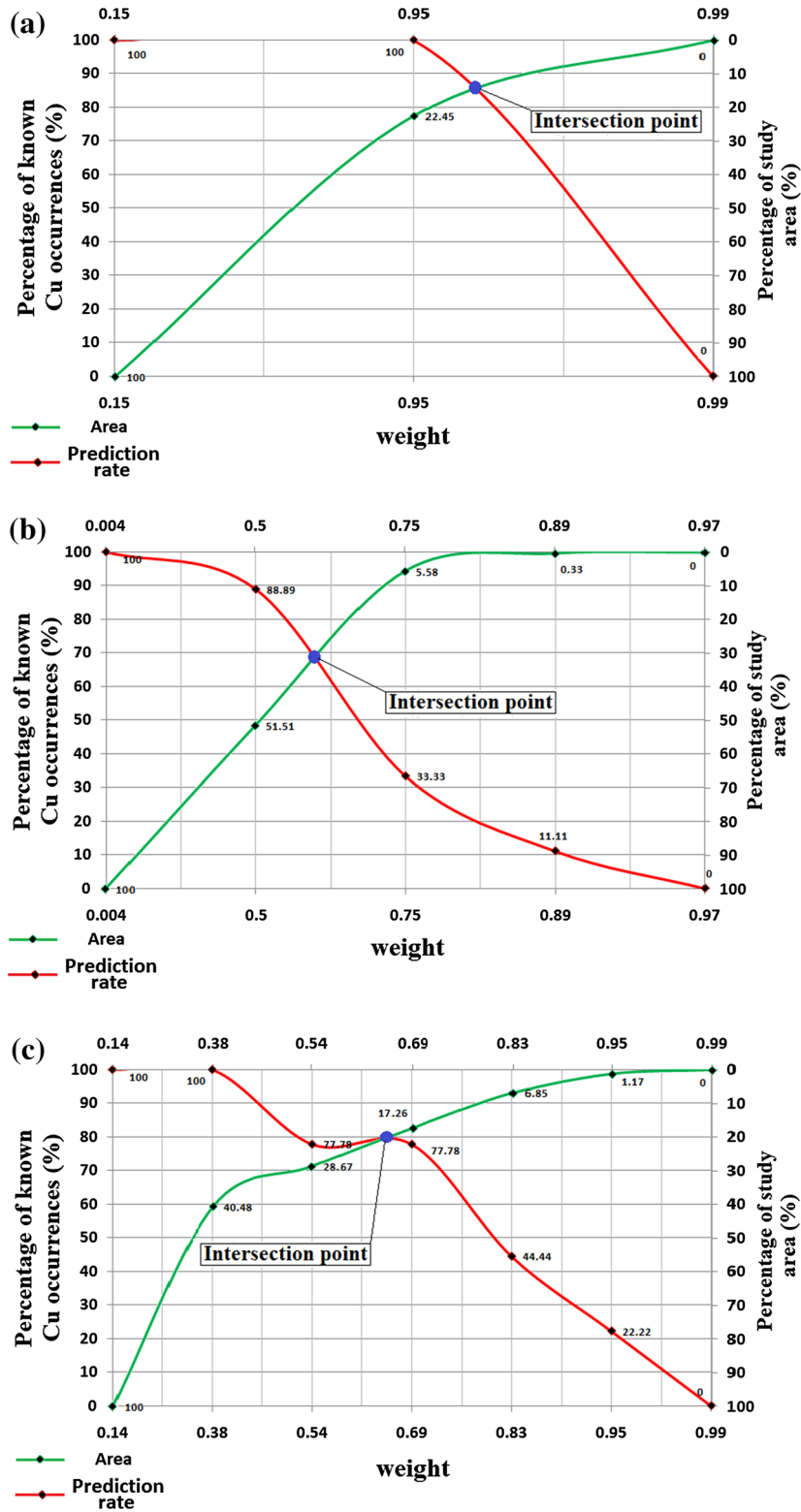
Figure 5. Prediction-area (P-A) plot for the classified weighted map of (a) distances to intrusive contacts, (b) multi-element geochemical signature, map of GMPI$_{Cu\text{-}porphyry}$ values, and (c) fault density.

Table 1. The Extracted Parameters from Intersection Point of P-A Plots for Continuous Weighted Individual Evidence Layers in Figure 5a–c

Evidence Layer	Prediction Rate (%)	Threshold for Binary Classification	Occupied Area (%)
Intrusive contact	86	0.96	14
Fault density	80	0.65	20
GMPI	69	0.6	31

Integration of Weighted Evidential Maps

In MPM, weighted evidential maps are integrated with functions that allow using a map weight portraying the relative importance of each evidential map (Bonham-Carter 1994; Carranza 2008b; Porwal et al. 2003c, 2004, 2006). In this paper, the values in evidential maps were weighted continuously using a logistic function (Yousefi et al. 2012, 2013, 2014; Yousefi and Carranza 2015), whereas the weights of individual evidential maps were assigned using the proposed data-driven P-A plot. Therefore, mathematical integration models that consider both the above-mentioned weights can be adapted for generating target areas. For this, we adapted the index overlay model proposed by Bonham-Carter (1994). Furthermore, to demonstrate the ability of the P-A plot in evaluating different prospectivity models and making binary maps, we used the Boolean logic model (Bonham-Carter 1994; Carranza 2008b) for the purpose of comparing results.

Data-Driven Multi-index Overlay

Multi-class index overlay is traditionally applied to knowledge-driven MPM (Bonham-Carter 1994; Chico-Olmo et al. 2002; Billa et al. 2004; Carranza 2008b) whereby evidential maps are categorized into some arbitrary classes, and are then integrated considering weights subjectively assigned to each evidential map. Each of the jth classes of the ith evidential map is assigned a score S_{ij} according to their relative importance. The relative importance of an evidential map compared to each of the other evidential maps is controlled by the assigned weights W_i. Weighted evidential maps are then combined using the following equation, which calculates an average weighted score ($\bar{S}$) for each pixel (Bonham-Carter 1994):

$$\bar{S} = \frac{\sum_{i}^{n} S_{ij} W_i}{\sum_{i}^{n} W_i}$$

Equation [1] is used to integrate classified evidential maps in knowledge-driven MPM (Bonham-Carter 1994; Carranza 2008b). Here, continuous values in evidential maps are weighted without using the locations of known mineral occurrences, and without using the expert judgment in discretization of evidential values into arbitrary classes (Yousefi et al. 2012, 2013, 2014; Yousefi and Carranza 2015). The weights of individual evidential maps are assigned considering their ability to predict mineral occurrences based on the P-A plot. Thus, although the choice of which datasets and mathematical functions to use is always knowledge-driven, Eq. [1] can be adapted as a data-driven multi-index overlay model as follows:

$$\text{DM}_{\text{IO}} = \frac{\sum_{i}^{n} W_{vi} W_i}{\sum_{i}^{n} W_i}, \tag{2}$$

where for every pixel in the study area, DM_{IO} is the data-driven multi-index overlay score, W_i is the weight of individual evidential layer i, assigned using P-A plot. The W_{vi} is pixel value in evidential layer i assigned continuously by using a logistic function (Yousefi et al. 2012, 2013, 2014). For the present study, Eq. [2] is written as follows:

$$\text{DM}_{\text{IO}} = \frac{WV_{\text{FD}} W_{\text{FD}} + WV_{\text{GMPI}} W_{\text{GMPI}} + WV_{\text{int}} W_{\text{int}}}{W_{\text{FD}} + W_{\text{GMPI}} + W_{\text{int}}}, \tag{3}$$

where W_{FD}, W_{GMPI}, and W_{int} are, respectively, weights of evidence layers namely fault density (FD), GMPI, and intrusive contacts (int), which are
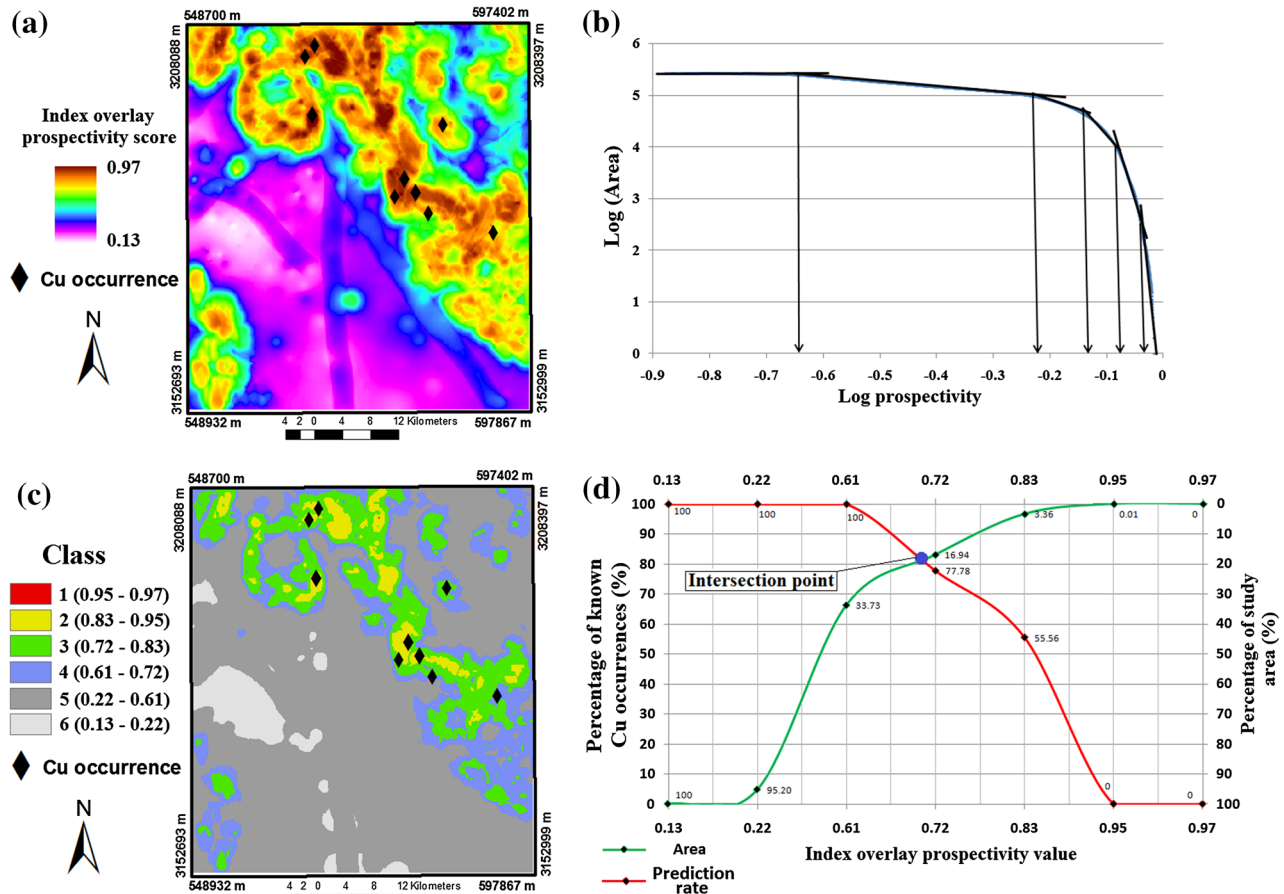
Figure 6. (a) Map of multi-index overlay prospectivity scores generated by combining continuous weighted maps of fault density (Fig. 2c), multi-element geochemical signature (GMPI$_{Cu\text{-}porphyry}$, Fig. 2b), and distances to intrusive contacts (Fig. 2a) using the Eq. [3]. (b) Concentration-area model, log–log plots for multi-index overlay prospectivity values in (a). (c) Classified multi-index overlay prospectivity map. (d) Prediction-area (P-A) plot for the classified multi-index overlay prospectivity model in (c).

assigned based on their respective P-A plot (Fig. 5a–c). In Eq. [3], WV_{FD}, WV_{GMPI}, and WV_{int} are the weights of evidential values of pixels in the corresponding evidence maps that are assigned continuously using a logistic function (Yousefi et al. 2012, 2013, 2014; Yousefi and Carranza 2015). The data-driven multi-index overlay prospectivity model for porphyry-Cu deposit generated using Eq. [3] is shown in Figure 6a.

Data-Driven Boolean Logic Modeling

Boolean logic modeling is also traditionally applied to knowledge-driven MPM (Bonham-Carter 1994; Harris et al. 2001; Carranza 2008b), whereby

attributes or classes of attributes of spatial data that meet a prospectivity recognition criterion are labeled TRUE (or given a class score of 1), otherwise they are labeled FALSE (or given a class score of 0). The class scores of 0 and 1 in a Boolean evidential map are only symbolic and non-numeric. Boolean evidential maps are combined logically using Boolean operators (AND, OR, NOT, XOR, etc.) in GIS-based knowledge-driven MPM (Bonham-Carter 1994; Thiart and De Wit 2000; Harris et al. 2001; Carranza 2008b). The output of combining evidential maps via Boolean logic modeling is a map with two classes, one class represent locations where all or most of the prospectivity recognition criteria are satisfied, while the other class represents locations where none of the prospectivity recognition criteria
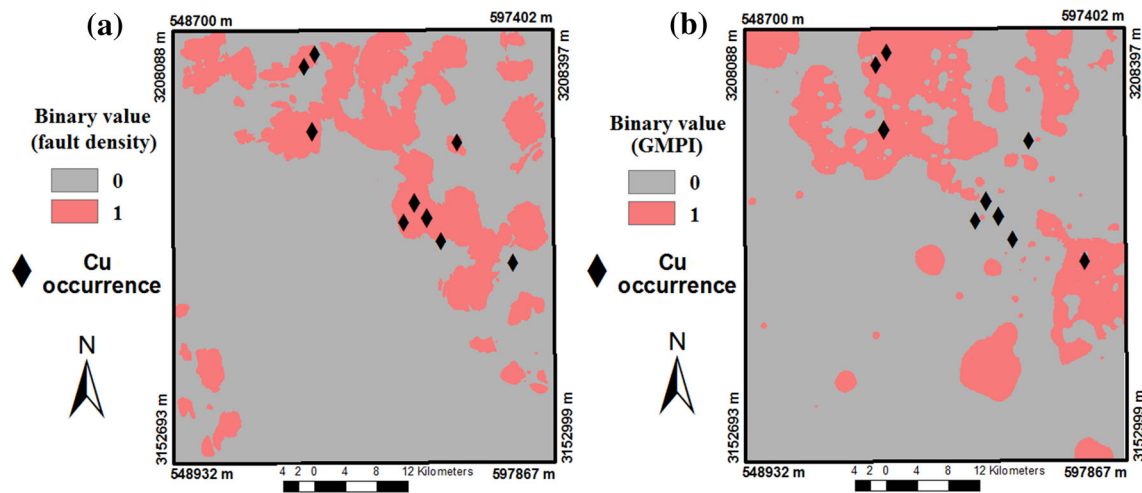
Figure 7. Binary evidential map of (a) fault density, and (b) geochemical multi-element signature, GMPI$_{Cu-porphyry}$.
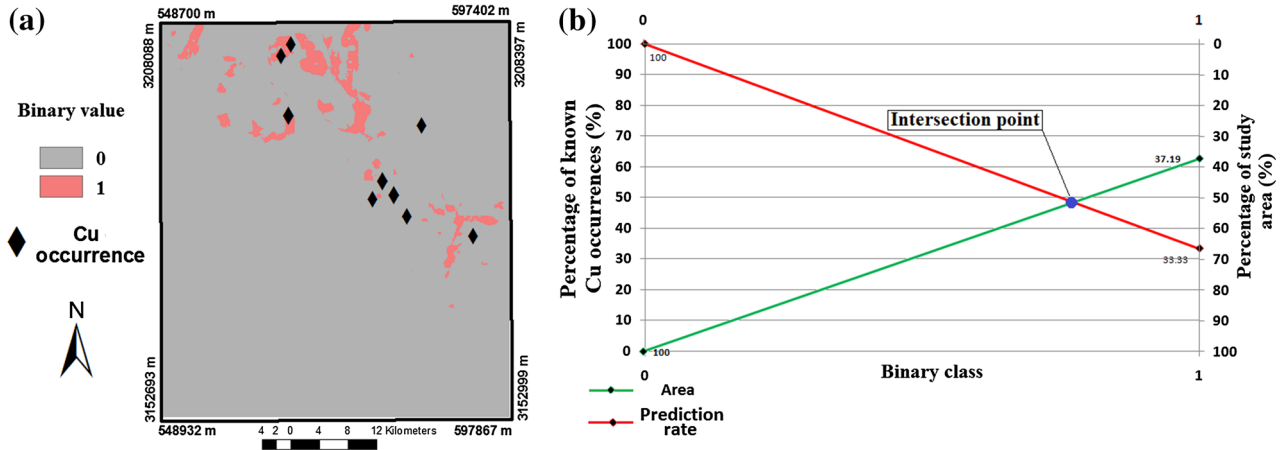

Figure 8. (a) Data-driven Boolean logic prospectivity model generated using AND operator by combining binary maps of fault density (Fig. 7a), multi-element geochemical signature (GMPI$_{Cu-porphyry}$, Fig. 7b), and distances to intrusive contacts (Fig. 4a). (b) Prediction-area (P-A) plot for the Boolean logic prospectivity model in (a).

is satisfied (Carranza 2008b). In the Boolean logic MPM method, the thresholds for generating binary maps are selected subjectively based on the expert judgment of analyst. Thus, there lies a problem of exploration bias arising from subjective expert judgment. Here, based on the purpose of this paper, threshold values for generating binary evidential maps are calculated by using the X values of intersection points in the P-A plots of individual evidential maps (Fig. 5a–c; Table 1). The binary evidential maps generated using the P-A plots are shown in Figure 7a, b for geochemical and fault density evidential maps. The binary evidential map of distances to intrusive contact is the same as Figure 4a. This is

because based on the P-A plot of distances to intrusive contacts the threshold value for binary classification is approximately 0.96, which is equal to the threshold obtained by the log–log plot of the C-A model in Figure 3a. The binary evidential maps (Figs. 4a, 7a, b) were integrated using the AND operator to make a data-driven Boolean logic prospectivity model for porphyry-Cu deposit (Fig. 8a).

Evaluation of the Models

After generation of two prospectivity models, data-driven multi-index overlay and data-driven

Boolean logic models, the locations of nine known porphyry-Cu occurrences in the study area were used as testing points in the P-A plots to evaluate the results. Therefore, the association of known mineral deposits with different classes of a prospectivity model is evaluated by overlaying the locations of known mineral deposits on a classified model (e.g., Carranza et al. 2005; Porwal et al. 2003c, 2004, 2006; Yousefi et al. 2012, 2013, 2014; Yousefi and Carranza 2015). For this, we used the C-A model (Figs. 6b) proposed by Cheng et al. (1994) to determine threshold prospectivity values for classification of the multi-index overlay prospectivity model (Fig. 6a). Based on Figure 6b, we classified the multi-index overlay prospectivity model (Fig. 6c) and then the P-A plot (Fig. 6d) for this model was created. For the Boolean logic prospectivity model (Fig. 8a), because there are two classes, the P-A plot was directly drown (Fig. 8b).

The intersection point in the P-A plot (Fig. 6d) for the multi-index overlay prospectivity model is higher than the intersection point in the P-A plot (Fig. 8b) for the Boolean logic prospectivity model. Based on the intersection points in Figure 6d, the multi-index overlay prospectivity model (Fig. 6a) predicts 19% of the study area as prospective in which 81% of the known porphyry-Cu occurrences are delineated, whereas based on the intersection points in Figure 8d the Boolean logic prospectivity model (Fig. 8a) predicts 51% of the study area as prospective in which 49% of the know porphyry-Cu occurrences are delineated. This comparison illustrates that target areas with high prospectivity values based on the multi-index overlay prospectivity model have priority for further exploration compared to target areas based on the Boolean logic prospectivity model. Thus, multi-index overlay prospectivity modeling is much better than Boolean logic prospectivity modeling in the study area.

DISCUSSION

The characteristics of a certain type of mineral deposits can be different in different areas. Such differences, which are a function of the relative importance of individual factors of mineralization in different areas, are related to geological features associated to mineralization. However, there are several geological features near and around mineralized areas and not all of them have the same priority of evidence for the deposit-type sought. In this

regard, we propose the P-A plot for efficient evaluation of the ability and relative importance of individual evidential maps to predict prospectivity for the deposit-type sought in a study area. Thus, the weight of individual evidential maps can be defined using the P-A plot for fuzzy logic and the AHP techniques for MPM (De Araújo and Macedo 2002; Moreira et al. 2003; Porwal et al. 2003c, 2004, 2006; Hosseinali and Alesheikh 2008; Najafi et al. 2014), in which weights of evidential maps must be defined for in the application of mathematical integration models. The P-A plot is a worthy tool for recognizing the efficiency of evidential maps. This shows, however, that because there are many mathematical models for integrating weighted evidential maps (e.g., Bonham-Carter 1994; Carranza 2008b), Carranza (2008b) mentioned that at least two mineral prospectivity models should be generated and compared to select more reliable target areas. For this, although field observations can be used to evaluate target areas predicted by prospectivity models (e.g., Gholami et al. 2012; Yousefi and Carranza 2015), if in an area there are some known mineral occurrences, the P-A plot can be used not only to efficiently evaluate and compare different prospectivity models in terms of their ability to predict mineral occurrences with respect to the sizes of predicted target areas (Yousefi and Carranza 2015) but also to assign weight to individual evidential maps and to select thresholds for creating binary predictor maps.

CONCLUDING REMARKS

The main findings of this study are as follows:

1. Using the P-A plot, introduced in this paper, individual evidential maps are weighted in a data-driven way, and it can be used to efficiently evaluate the relative importance of individual evidential maps.
2. The P-A plot is useful for defining threshold evidence values for creating binary evidential maps.
3. The data-driven techniques of multi-index overlay and Boolean logic modeling proposed in this paper avoid subjective opinion for (a) discretization of evidential values into some arbitrary classes and (b) assignment of weights to individual evidential maps. Therefore, using the proposed techniques,

introduction of systemic bias in mineral prospectivity mapping can be avoided or reduced.

ACKNOWLEDGMENTS

REFERENCES

Afzal, P., Fadakar Alghalandis, Y., Khakzad, A., Moarefvand, P., & Rashidnejad Omran, N. (2011). Delineation of mineralization zones in porphyry Cu deposits by fractal concentration–volume modeling. *Journal of Geochemical Exploration, 108*, 220–232.

Agard, P., Omrani, J., Jolivet, L., & Mouthereau, F. (2005). Convergence history across Zagros (Iran): Constraints from collisional and earlier deformation. *International Journal of Earth Sciences, 94*, 401–419.

Agterberg, F. P. (2007). Mixtures of multiplicative cascade models in geochemistry. *Nonlinear Processes in Geophysics, 14*, 201–209.

Alavi, M. (1980). Tectonostratigraphic evolution of the Zagrosides of Iran. *Geology, 8*, 144–149.

Arias, M., Gumiel, P., Sanderson, D. J., & Martin-Izard, A. (2011). A multifractal simulation model for the distribution of VMS deposits in the Spanish segment of the Iberian Pyrite Belt. *Computers & Geosciences, 37*, 1917–1927.

Arribas, A. J. (1995). Contemporaneous formation of adjacent porphyry and epithermal Cu-Au deposits over 300 ka in northern Luzon, Philippines. *Geology, 23*, 337–340.

Atapour, H., & Aftabi, A. (2007). The geochemistry of gossans associated with Sarcheshmeh porphyry copper deposit, Rafsanjan, Kerman, Iran: Implications for exploration and the environment. *Journal of Geochemical Exploration, 93*, 47–65.

Bayes, T. (1764). An essay toward solving a problem in the doctrine of chances. *Philosophical Transactions of the Royal Society of London, 53*, 370–418.

Berberian, F., & Berberian, M. (1981). Tectono-plutonic episodes in Iran. In H.K. Gupta, & F.M. Delany (Eds.), *Zagroz–Hindu Kush–Himalaya Geodynamic Evolution* (pp. 5–32). Washington: American Geophysical Union & Geological Society of America.

Berberian, F., Muir, I. D., Pankhurst, R. J., & Berberian, M. (1982). Late Cretaceous and Early Miocene Andean-type plutonic activity in northern Makran and central Iran. *Journal of the Geological Society of London, 139*, 605–614.

Billa, M., Cassard, D., Lips, A. L. W., Bouchot, V., Tourliére, B., Stein, G., & Guillou-Frottier, L. (2004). Predicting gold-rich epithermal and porphyry systems in the central Andes with a continental-scale metallogenic GIS. *Ore Geology Reviews, 25*, 39–67.

Bonham-Carter, G. F. (1994). *Geographic information systems for geoscientists: Modelling with GIS*. Oxford: Pergamon.

Bonham-Carter, G. F., Agterberg, F. P., & Wright, D. F. (1989). Weights of evidence modelling: A new approach to mapping mineral potential. In F. P. Agterberg & G. F. Bonham-Carter (Eds.), *Statistical applications in the earth sciences*, Geological Survey of Canada, Paper 89-9 (pp. 171–183).

Boomeri, M., Nakashima, K., & Lentz, D. R. (2009). The Miduk porphyry Cu deposit, Kerman, Iran: A geochemical analysis of the potassic zone including halogen element systematics related to Cu mineralization processes. *Journal of Geochemical Exploration, 103*, 17–29.

Carranza, E. J. M. (2004). Weights of evidence modeling of mineral potential: A case study using small number of prospects, Abra, Philippines. *Natural Resources Research, 13*, 173–187.

Carranza, E. J. M. (2008a). Controls on mineral deposit occurrence inferred from analysis of their spatial pattern and spatial association with geological features. *Ore Geology Reviews, 35*, 383–400.

Carranza, E. J. M. (2008b). Geochemical anomaly and mineral prospectivity mapping in GIS. In *Handbook of exploration and environmental geochemistry* (Vol. 11, p. 351). Amsterdam: Elsevier.

Carranza, E. J. M. (2009). Improved wildcat modeling of mineral prospectivity. *Resource Geology, 60*, 129–149.

Carranza, E. J. M. (2010a). Catchment basin modelling of stream sediment anomalies revisited: Incorporation of EDA and fractal analysis. *Geochemistry: Exploration, Environment, Analysis, 10*, 365–381.

Carranza, E. J. M. (2010b). Mapping of anomalies in continuous and discrete fields of stream sediment geochemical landscapes. *Geochemistry: Exploration, Environment, Analysis, 10*, 171–187.

Carranza, E. J. M. (2011). Analysis and mapping of geochemical anomalies using logratio-transformed stream sediment data with censored values. *Journal of Geochemical Exploration, 110*, 167–185.

Carranza, E. J. M., & Hale, M. (2001). Geologically-constrained fuzzy mapping of gold mineralization potential, Baguio district, Philippines. *Natural Resources Research, 10*, 125–136.

Carranza, E. J. M., & Hale, M. (2002a). Where are porphyry copper deposits spatially localized? A case study in Benguet province, Philippines. *Natural Resources Research, 11*, 45–59.

Carranza, E. J. M., & Hale, M. (2002b). Wildcat mapping of gold potential, Baguio district, Philippines. *Transactions of the Institution of Mining and Metallurgy (Section B: Applied Earth Science), 111*, 100–105.

Carranza, E. J. M., Hale, M., & Faassen, C. (2008a). Selection of coherent deposit-type locations and their application in data-driven mineral prospectivity mapping. *Ore Geology Reviews, 33*, 536–558.

Carranza, E. J. M., van Ruitenbeek, F. J. A., Hecker, C., van der Meijde, M., & van der Meer, F. D. (2008b). Knowledge-guided data-driven evidential belief modeling of mineral prospectivity in Cabo de Gata, SE Spain. *International Journal of Applied Earth Observation and Geoinformation, 10*, 374–387.

Carranza, E. J. M., Owusu, E., & Hale, M. (2009). Mapping of prospectivity and estimation of number of undiscovered prospects for lode-gold, southwestern Ashanti Belt, Ghana. *Mineralium Deposita, 44*, 915–938.

Carranza, E. J. M., & Sadeghi, M. (2010). Predictive mapping of prospectivity and quantitative estimation of undiscovered VMS deposits in Skellefte district (Sweden). *Ore Geology Reviews, 38*, 219–241.

Carranza, E. J. M., & Sadeghi, M. (2014). Post-VMS mineralization deformations (1.88–1.82 Ga) of the Skellefte district (Sweden): Insights from the spatial pattern of VMS occurrences. *Frontiers of Earth Science, 8*, 319–324.

Carranza, E. J. M., Woldai, T., & Chikambwe, E. M. (2005). Application of data-driven evidential belief functions to prospectivity mapping for aquamarine-bearing pegmatites, Lundazi district, Zambia. *Natural Resources Research, 14*, 47–63.

Chen, Z., Zhang, L., Wan, B., Wu, H., & Cleven, N. (2011). Geochronology and geochemistry of the Wunugetushan porphyry Cu–Mo deposit in NE china, and their geological significance. *Ore Geology Reviews, 43*, 92–105.

Cheng, Q. (1995). The perimeter-area fractal model and its application to geology. *Mathematical Geology, 27*, 69–82.

Cheng, Q. (1999). Multifractality and spatial statistics. *Computers & Geosciences, 25*, 949–961.

Cheng, Q. (2007). Mapping singularities with stream sediment geochemical data for prediction of undiscovered mineral deposits in Gejiu, Yunnan Province, China. *Ore Geology Reviews, 32*, 314–324.

Cheng, Q., & Agterberg, F. P. (1995). Multifractal modeling and spatial point processes. *Mathematical Geology, 27*, 831–845.

Cheng, Q., & Agterberg, F. P. (2009). Singularity analysis of ore-mineral and toxic trace elements in stream sediments. *Computers & Geosciences, 35*, 34–244.

Cheng, Q., Agterberg, F. P., & Ballantyne, S. B. (1994). The separation of geochemical anomalies from background by fractal methods. *Journal of Geochemical Exploration, 51*, 109–130.

Cheng, Q., Agterberg, F. P., & Bonham-Carter, G. F. (1996). A spatial analysis method for geochemical anomaly separation. *Journal of Geochemical Exploration, 56*, 183–195.

Cheng, Q., Xia, Q., Li, W., Zhang, S., Chen, Z., Zuo, R., & Wang, W. (2010). Density/area power law models for separating multi-scale anomalies of ore and toxic elements in stream sediments in Gejiu mineral district, Yunnan Province, China. *Biogeosciences, 7*, 3019–3025.

Chico-Olmo, M., Abarca, F., & Rigol, J. P. (2002). Development of a decision support system based on remote sensing and GIS techniques for gold-rich area identification in SE Spain. *International Journal of Remote Sensing, 23*, 4801–4814.

De Araújo, C. C., & Macedo, A. B. (2002). Multicriteria geologic data analysis for mineral favorability mapping: Application to a metal sulphide mineralized area, Ribeira Valley metallogenic province, Brazil. *Natural Resources Research, 11*, 29–43.

Deng, J., Wang, Q. F., Wan, L., Liu, H., Yang, L. Q., & Zhang, J. (2011). A multifractal analysis of mineralization characteristics of the Dayingezhuang disseminated-veinlet gold deposit in the Jiaodong gold province of China. *Ore Geology Reviews, 40*, 54–64.

Deng, J., Wang, Q., Wan, L., Yang, L., Gong, Q., Zhao, J., & Liu, H. (2009). Self-similar fractal analysis of gold mineralization of Dayingezhuang disseminated-veinlet deposit in Jiaodong gold province, China. *Journal of Geochemical Exploration, 102*, 95–102.

Deng, J., Wang, Q., Yang, L., Wang, Y., Gong, Q., & Liu, H. (2010). Delineation and explanation of geochemical anomalies using fractal models in the Heqing area, Yunnan Province, China. *Journal of Geochemical Exploration, 105*, 95–105.

Ford, A., & Blenkinsop, T. G. (2008). Evaluating geological complexity and complexity gradients as controls on copper mineralization, Mt Isa Inlier. *Australian Journal of Earth Sciences, 55*, 13–23.

Ford, A., & Blenkinsop, T. G. (2009). An expanded de Wijs model for multifractal analysis of mineral production data. *Mineralium Deposita, 44*, 233–240.

Ghasemi, A., & Talbot, C. J. (2006). A new tectonic scenario for the Sanandaj–Sirjan Zone (Iran). *Journal of Asian Earth Sciences, 26*, 683–693.

Gholami, R., Moradzadeh, A., & Yousefi, M. (2012). Assessing the performance of independent component analysis in remote sensing data processing. *Journal of the Indian Society of Remote Sensing, 40*, 577–588.

Good, I. J. (1950). *Probability and the weighting of evidence*. London: Griffin. 119p.

Grabeljsek, V. (1956). Geological Map of Sabzevaran (1:100,000), Geological Survey of Iran publication.

Guillou-Frottier, L., & Burov, E. (2003). The development and fracturing of plutonic apexes: Implications for porphyry ore deposits. *Earth and Planetary Science Letters, 214*, 341–356.

Gumiel, P., Sanderson, D. J., Arias, M., Roberts, S., & Martin-Izard, A. (2010). Analysis of the fractal clustering of ore deposits in the Spanish Iberian Pyrite Belt. *Ore Geology Reviews, 38*, 307–318.

Hanuš, V., Vaněk, J., & Špičák, A. (2000). Seismically active fracture zones and distribution of large accumulations of metals in the central part of Andean South America. *Mineralium Deposita, 35*, 2–20.

Harris, J. R., Wilkinson, L., Heather, K., Fumerton, S., Bernier, M. A., Ayer, J., & Dahn, R. (2001). Application of GIS processing techniques for producing mineral prospectivity maps—A case study: Mesothermal Au in the Swayze Greenstone Belt, Ontario, Canada. *Natural Resources Research, 10*, 91–124.

Hengl, T. (2006). Finding the right pixel size. *Computers & Geosciences, 32*, 1283–1298.

Hezarkhani, A. (2006a). Mineralogy and fluid inclusion investigations in the Reagan Porphyry System, Iran, the path to an uneconomic porphyry copper deposit. *Journal of Asian Earth Sciences, 27*, 598–612.

Hezarkhani, A. (2006b). Petrology of the intrusive rocks within the Sungun Porphyry Copper Deposit, Azerbaijan, Iran. *Journal of Asian Earth Sciences, 27*, 326–340.

Hezarkhani, A. (2009). Hydrothermal fluid geochemistry at the Chah-Firuzeh porphyry copper deposit, Iran: Evidence from fluid inclusions. *Journal of Geochemical Exploration, 101*, 254–264.

Hosseinali, F., & Alesheikh, A. A. (2008). Weighting spatial information in GIS for copper mining exploration. *American Journal of Applied Sciences, 5*, 1187–1198.

Jaccard, P. (1908). Nouvelles recherché sur la distribution florale. *Bulletin Societe Vaudoise des Sciences Naturelles, 44*, 223–270.

Lindsay, M., Betts, P. G., & Ailleres, L. (2014). Data fusion and porphyry copper prospectivity models, southeastern Arizona. *Ore Geology Reviews, 61*, 120–140.

Lisitsin, V. A., González-Álvarez, I., & Porwal, A. (2013). Regional prospectivity analysis for hydrothermal-remobilised nickel mineral systems in western Victoria, Australia. *Ore Geology Reviews, 52*, 100–112.

Lusty, P. A. J., Scheib, C., Gunn, A. G., & Walker, A. S. D. (2012). Reconnaissance-scale prospectivity analysis for gold mineralisation in the Southern Uplands-Down-Longford Terrane, Northern Ireland. *Natural Resources Research, 21*, 359–382.

Mandelbrot, B. B. (1977). *Fractals: Form, chance, and dimension*. San Francisco: Freeman. 365.

Mandelbrot, B. B. (1983). *The fractal geometry of nature, (updated and augmented edition)*. New York: Freeman. 468.

Mandelbrot, B. B., Passoja, D. E., & Paullay, A. J. (1984). Fractal character of fracture surfaces of metals. *Nature, 308*(5961), 721–722.

Meshkani, S. A., Mehrabi, B., Yaghubpur, A., & Sadeghi, M. (2013). Recognition of the regional lineaments of Iran: Using geospatial data and their implications for exploration of metallic ore deposits. *Ore Geology Reviews, 55*, 48–63.

Moreira, F. R. S., Almeida-Filho, R., & Câmara, G. (2003). Spatial analysis techniques applied to mineral prospecting: An evaluation in the Poços de Caldas Plateau. *Revista Brasileira de Geosciências, 33*(2-Suppl.), 183–190.

Najafi, A., Karimpour, M. H., & Ghaderi, M. (2014). Application of fuzzy AHP method to IOCG prospectivity mapping: A case study in Taherabad prospecting area, eastern Iran. *International Journal of Applied Earth Observation and Geoinformation, 33*, 142–154.

Nykänen, V., Groves, D. I., Ojala, V. J., Eilu, P., & Gardoll, S. J. (2008). Reconnaissance scale conceptual fuzzy-logic prospectivity modeling for iron oxide copper—Gold deposits in the northern Fennoscandian Shield, Finland. *Australian Journal of Earth Sciences, 55*, 25–38.

Omrani, J., Agard, P., Whitechurch, H., Benoit, M., Prouteau, G., & Jolivet, L. (2008). Arc-magmatism and subduction history beneath the Zagros Mountains, Iran: A new report of adakites and geodynamic consequences. *Lithos, 106*, 380–398.

Panahi, A., & Cheng, Q. (2004). Multifractality as a measure of spatial distribution of geochemical patterns. *Mathematical Geology, 36*, 827–846.

Pazand, K., Hezarkhani, A., Ataei, M., & Ghanbari, Y. (2011). Combining AHP with GIS for predictive Cu porphyry potential mapping: A case study in Ahar area (NW, Iran). *Natural Resources Research, 20*, 251–262.

Pirajno, F. (2010). Intracontinental strike-slip faults, associated magmatism, mineral systems and mantle dynamics: Examples from NW China and Altay-Sayan (Siberia). *Journal of Geodynamics, 50*, 325–346.

Porwal, A., Carranza, E. J. M., & Hale, M. (2003a). Extended weights-of-evidence modelling for predictive mapping of base metal deposit potential in Aravalli province, western India. *Exploration and Mining Geology, 10*, 155–163.

Porwal, A., Carranza, E. J. M., & Hale, M. (2003b). Artificial neural networks for mineral potential mapping: A case study from Aravalli Province, Western India. *Natural Resources Research, 12*, 155–171.

Porwal, A., Carranza, E. J. M., & Hale, M. (2003c). Knowledge-driven and data-driven fuzzy models for predictive mineral potential mapping. *Natural Resources Research, 12*, 1–25.

Porwal, A., Carranza, E. J. M., & Hale, M. (2004). A hybrid neuro-fuzzy model for mineral potential mapping. *Mathematical Geology, 36*, 803–826.

Porwal, A., Carranza, E. J. M., & Hale, M. (2006). A hybrid fuzzy weights-of-evidence model for mineral potential mapping. *Natural Resources Research, 15*, 1–14.

Qu, X., Hou, Z., Zaw, K., & Youguo, L. (2007). Characteristics and genesis of Gangdese porphyry copper deposits in the southern Tibetan Plateau: Preliminary geochemical and geochronological results. *Ore Geology Reviews, 31*, 205–223.

Raines, G. L. (2008). Are fractal dimensions of the spatial distribution of mineral deposits meaningful? *Natural Resource Research, 17*, 87–97.

Rogge, D. M., Halden, N. M., & Beaumont-Smith, C. (2006). Application of data integration for shear hosted Au potential modeling: Lynn Lake Greenstone Belt, Northwestern Manitoba, Canada. In J. R. Harris (Ed.), *GIS for the earth sciences: Geological Association of Canada Special Publication 44* (pp. 191–210). St. John's: Geological Association of Canada.

Roy, R., Cassard, D., Cobbold, P. R., Rossello, E. A., Billa, M., Bailly, L., & Lips, A. L. W. (2006). Predictive mapping for copper–gold magmatic-hydrothermal systems in NW Argentina: Use of a regional-scale GIS, application of an expert-guided data-driven approach, and comparison with results from a continental-scale GIS. *Ore Geology Reviews, 29*, 260–286.

Sengor, A. M. C., Altiner, D., Cin, A., Ustomer, T., & Hsu, K. J. (1988). The origin and assembly of the Tethyside orogenic collage at the expense of Gondwana land. In M. G. Audley-Charles & A. Hallam (Eds.), *Gondwana and Tethys. Geological Society*, (pp. 119–181). London: Special Publication, Geological Society.

Sillitoe, R. H. (1997). Characteristics and controls of the largest porphyry copper–gold and epithermal gold deposits in the circum-Pacific region. *Australian Journal of Earth Sciences, 44*, 373–388.

Sillitoe, R. H. (2010). Porphyry copper systems. *Economic Geology, 105*, 3–41.

Singer, D. A., Berger, V. I., & Moring, B. C. (2005). Porphyry copper deposits of the world: Database, map, grade and tonnage models. U.S. Geological Survey. Open-File Report (pp. 1005–1060).

Storti, F., Holdsworth, R. E., & Salvini, F. (2003). Intraplate strike-slip deformation belts. *Geological Society, London, Special Publication, 210*, 1–14.

Takin, M. (1972). Iranian geology and continental drift in the Middle East. *Nature, 235*, 147–150.

Tangestani, M. H., & Moore, F. (2002a). Porphyry copper alteration mapping in the Meiduk area, Iran. *International Journal of Remote Sensing, 23*, 4815–4825.

Tangestani, M. H., & Moore, F. (2002b). The use of Dempster-Shafer model and GIS in integration of geoscientific data for porphyry copper potential mapping, north of Shahr-e-Babak, Iran. *International Journal of Applied Earth Observation and Geoinformation, 4*, 65–74.

Thiart, C., & De Wit, M. (2000). Linking spatial statistics to GIS: Exploring potential gold and tin models of Africa. *South African Journal of Geology, 103*, 215–230.

Wang, Z., Cheng, Q., Cao, L., Xia, Q., & Chen, Z. (2006). Fractal modelling of the microstructure property of quartz mylonite during deformation process. *Mathematical Geology, 39*, 53–68.

Wang, Z., Cheng, Q., Xu, D., & Dong, Y. (2008). Fractal modeling of sphalerite banding in Jinding Pb–Zn deposit, Yunnan, Southwestern China. *Journal of China University Geosciences, 19*, 77–84.

Wang, Q., Deng, J., Wan, L., & Zhang, Z. (2011a). Fractal analysis of the ore-forming process in a skarn deposit: A case study in the Shizishan area, China. In A. N. Sial, Bettencourt, J. S., De Campos, C. P., Ferreira, V. P. (Eds.), *Granite-related ore deposits: Geological Society, London, Special Publications* (Vol. 350, pp. 89–104).

Wang, G., Zhang, S., Yan, C., Song, Y., Sun, Y., Li, D., & Xu, F. (2011b). Mineral potential targeting and resource assessment based on 3D geological modeling in Luanchuan region, China. *Computers & Geosciences, 37*, 1976–1988.

Yousefi, M., & Carranza, E. J. M. (2015). Fuzzification of continuous-value spatial evidence for mineral prospectivity mapping. *Computers & Geosciences, 74*, 97–109.

Yousefi, M., Carranza, E. J. M., & Kamkar-Rouhani, A. (2013). Weighted drainage catchment basin mapping of stream sediment geochemical anomalies for mineral potential mapping. *Journal of Geochemical Exploration, 128*, 88–96.

Yousefi, M., Kamkar-Rouhani, A., & Carranza, E. J. M. (2012). Geochemical mineralization probability index (GMPI): A new approach to generate enhanced stream sediment geochemical evidential map for increasing probability of success in mineral potential mapping. *Journal of Geochemical Exploration, 115*, 24–35.

Yousefi, M., Kamkar-Rouhani, A., & Carranza, E. J. M. (2014). Application of staged factor analysis and logistic function to create a fuzzy stream sediment geochemical evidence layer for mineral prospectivity mapping. *Geochemistry: Exploration, Environmental, Analysis, 14*, 45–58.

Yule, G. U. (1912). On the methods of measuring association between two attributes. *Journal of the Royal Statistical Society, 75*, 579–642.

Zhao, J., Chen, S., Zuo, R., & Carranza, E. J. M. (2011). Mapping complexity of spatial distribution of faults using fractal and multifractal models: Vectoring towards exploration targets. *Computers & Geosciences, 37*, 1958–1966.

Ziaii, M., Carranza, E. J. M., & Ziaei, M. (2011). Application of geochemical zonality coefficients in weights-of-evidence modeling of mineral prospectivity. *Computers & Geosciences, 37*, 1935–1945.

Zuo, R. (2011a). Decomposing of mixed pattern of arsenic using fractal model in Gangdese belt, Tibet, China. *Applied Geochemistry, 26*, S271–S273.

Zuo, R. (2011b). Identifying geochemical anomalies associated with Cu and Pb\Zn skarn mineralization using principal component analysis and spectrum–area fractal modeling in the Gangdese Belt, Tibet (China). *Journal of Geochemical Exploration, 111*, 13–22.

Zuo, R. (2011c). Regional exploration targeting model for Gangdese porphyry copper deposits. *Resource Geology, 61*, 296–303.

Zuo, R., Agterberg, F. P., Cheng, Q., & Yao, L. (2009a). Fractal characterization of the spatial distribution of geological point processes. *International Journal of Applied Earth Observation and Geoinformation, 11*, 394–402.

Zuo, R., & Cheng, Q. (2008). Mapping singularities: A technique to identify potential Cu mineral deposits using sediment geochemical data, an example for Tibet, west China. *Mineralogical Magazine, 72*, 531–534.

Zuo, R., Cheng, Q., Agterberg, F. P., & Xia, Q. (2009b). Application of singularity mapping technique to identify local anomalies using stream sediment geochemical data, a case study from Gangdese, Tibet, western China. *Journal of Geochemical Exploration, 101*, 225–235.

Zuo, R., & Xia, Q. (2009). Application fractal and multifractal methods to mapping prospectivity for metamorphosed sedimentary iron deposits using stream sediment geochemical data in eastern Hebei province, China. *Geochimica et Cosmochimica Acta, 73*, A1540–A1540.